Journal of Asian Earth Sciences 115 (2016) 298–307

Contents lists available at ScienceDirect

Journal of Asian Earth Sciences

journal homepage: www.elsevier.com/locate/jseaes

Drought reconstruction in eastern Hulun Buir steppe, China and its linkages to the sea surface temperatures in the Pacific Ocean

Na Liu [a,c], Yu Liu [b,a], Guang Bao [c,b,*], Ming Bao [d], Yanchao Wang [e], Lizhi Zhang [f], Yuxiang Ge [f], Wurigen Bao [f], Heng Tian [f]

[a] School of Human Settlements and Civil Engineering, Xi'an Jiaotong University, Xi'an 710049, China
[b] State Key Laboratory of Loess and Quaternary Geology, Institute of Earth Environment, Chinese Academy of Sciences, Xi'an 710075, China
[c] Shaanxi Key Laboratory of Disaster Monitoring and Mechanism Simulating, College of Geography and Environment, Baoji University of Arts and Sciences, Baoji 721013, China
[d] The Eleventh Middle School of Dalian Development Zone, Dalian 116635, China
[e] Department of Geography, Xingtai University, Xingtai 054001, China
[f] Honghuaerji Forestry Bureau of Inner Mongolia, Honghuaerji 021112, China

ARTICLE INFO

Article history:
Received 2 February 2015
Received in revised form 12 October 2015
Accepted 20 October 2015
Available online 20 October 2015

Keywords:
Hulun Buir steppe
Tree rings
Drought reconstruction
East Asian summer monsoon
PDO
ENSO

ABSTRACT

A tree-ring width chronology covering the period 1780–2013 AD was developed from *Pinus sylvestris* var. *mongolica* for the eastern Hulun Buir steppe, a region located on the edge of the eastern Mongolian Plateau, China. Climate-growth response analysis revealed drought stress to be the primary limiting factor for tree growth. Therefore, the mean February–July standardized precipitation evapotranspiration index (SPEI) was reconstructed over the period 1819–2013, where the reconstruction could account for 32.8% of the variance in the instrumental record over the calibration period 1953–2011. Comparison with other tree-ring-based moisture sequences from nearby areas confirmed a high degree of confidence in our reconstruction. Severe drought intervals since the late 1970s in our study area consisted with the weakening East Asian summer monsoon, which modulating regional moisture conditions in semi-arid zone over northern China. Drought variations in the study area significantly correlated with sea surface temperatures (SSTs) in North Pacific Ocean, suggesting a possible connection of regional hydroclimatic variations to the Pacific Decadal Oscillation (PDO). The potential influence associated with El Niño-Southern Oscillation (ENSO) was primarily analyzed.

1. Introduction

An amplification of the hydrological cycle, including increased frequency and severity of droughts, is a likely consequence of the global warming (e.g. Cook et al., 2004; Dai et al., 2004; Dai, 2011; Liu et al., 2014; Trenberth et al., 2004; Vicente-Serrano et al., 2010a, 2010b). Severe droughts have strong influence on agriculture, water resources and ecosystems (Dai, 2011), and are affecting the livelihood of millions of people around the world each year (Wilhite, 2000). Arid and semi-arid regions tend to be affected by this climate condition, including high-latitude Asia (Li et al., 2009). A prolonged four-year extreme drought from 1999 to 2002 occurred in the Mongolian Plateau (Davi et al., 2006, 2013; Pederson et al., 2013) and its vicinity (Bao et al., 2012, 2015; Zou et al., 2005) leading to huge economic and societal losses (Batima, 2006; Zhang and Gao, 2004). For example, in Inner Mongolia, China, the yield of crops (297×10^4 ha) and pasture (5733×10^4 ha) were significantly reduced during the harsh drought in 2001 (http://www.weather.com.cn/zt/kpzt/1244064.shtml). Another massive drought appeared in 2009, affecting 10.8×10^6 acres of farmland and resulting in severe drinking water shortage for 810,000 people drinking water difficulties in northeast China including eastern Inner Mongolia (http://www.chinadaily.com.cn/cndy/2009-08/13/content_8562996.htm). In 2014, the total drought area and that of the severest in Inner Mongolia covering 720,000 and 111,000 km^2, respectively (http://nmg.sina.com.cn/z/nmggh/index.shtml).

Hulun Buir city in the northeastern Inner Mongolia, locates at the borders between China, Russia and Mongolia. Natural grassland accounts for 80% of the entire 263,953 km^2 area of Hulun Buir city, and the steppe is the largest prairie in China. The weather in winter is very dry and severe due to the influence of the Siberian High, while in summer it is very warm and moist because of the

* Corresponding author at: Shaanxi Key Laboratory of Disaster Monitoring and Mechanism Simulating, College of Geography and Environment, Baoji University of Arts and Sciences, Baoji 721013, China
E-mail addresses: baoguang@ieecas.cn, baoguang23@163.com (G. Bao).

http://dx.doi.org/10.1016/j.jseaes.2015.10.009
1367-9120/

Asian summer monsoon (Chinese Academy of Sciences, 1984). The main extractive industry over this region includes livestock breeding and farming, which are particularly vulnerable to climate changes. The steppe ecosystems are quite fragile for cooperating effects exhibited by wind erosion, desertification, overgrazing and soil salinization (Shen, 2008; Wang et al., 2010). Like other regions in the Mongolian Plateau, the Hulun Buir steppe is also threatened by drought stress in the last decades (Bao et al., 2015; Chen et al., 2012; Li et al., 2009). However, short and sparse meteorological records (most back to 1950s) hamper us to well understand the processes and possible mechanisms of drought variations from a long perspective in this climate-sensitive region. Tree rings are one of the most useful climate proxies have proved their values of identifying the climate change characteristics according to the reliable relationships between tree-ring indices and climatic factors. Many studies based on tree rings have been conducted in Mongolia and surrounding areas, (e.g. Cook et al., 2010; D'Arrigo et al., 2000, 2001; Davi et al., 2006, 2009, 2010; Liang et al., 2007; Liu et al., 2009; Pederson et al., 2001, 2013). Nevertheless, studies obtained from the eastern edge of the Mongolian Plateau are still few (Bao, 2015; Bao et al., 2012, 2015; Chen et al., 2012; Liu et al., 2009). The purposes of our study are (1) to recover the mean February–July drought variability during the last two centuries for eastern Hulun Buir steppe, China, and (2) to identify the possible connections of drought fluctuations in eastern Mongolian Plateau with the sea surface temperatures (SSTs) in the remote Pacific Ocean.

2. Materials and methods

2.1. Study area and climate data

The study area is located in the eastern Hulun Buir steppe, China, a transitional zone between the Da Hinggan Mountains and the Mongolian Plateau (Fig. 1). This region lies in the boundary zone between arid and semi-arid conditions, monsoon and non-monsoon climate. The climate in the region is characterized by extreme temperature, strong winds, limited precipitation, high evaporation, and poor soil by wind erosion (Wang et al., 2010; Zhu et al., 2003).

Meteorological data of the monthly precipitation, monthly mean temperature and maximum temperature during the period of 1953–2012 from both Hailar (119°45′E, 49°13′N, 610 m a.s.l.) and Aershan (119°57′E, 47°10′N, 1027 m a.s.l.) stations were supplied by the China Meteorological Data Sharing Service System (http://cdc.cma.gov.cn). For the reason of effectively reducing the small-scale noise or stochastic components contained in single station (Bao et al., 2015; Chen et al., 2012; Davi et al., 2006), the arithmetical averaged data of Hailar and Aershan stations were applied to stand for regional climatic conditions and further analyses. The warmest and the coldest months are July (18.4 °C) and January (−25.6 °C), respectively. Annual mean temperature and total precipitation are −2.0 °C and 398.8 mm, respectively. The sum of precipitation from May to September is 332.4 mm, accounting for 83.3% of the total annual rainfall. Average monthly temperature and precipitation for the 1953–2012 period and May–September mean temperature and total precipitation are provided in Fig. 2.

Data of the Palmer drought severity index (PDSI) on a 2.5° × 2.5° grid (Dai et al., 2004) and the 0.5° × 0.5° grid standardized precipitation evapotranspiration index (SPEI) version 2.2 on 1 month time-scale were utilized in this study (Vicente-Serrano et al., 2010a, 2010b). The former is based on a soil moisture supply-and-demand model, which integrating cumulative effects of precipitation and temperature, the latter is designed to combine advantages of the multitemporal nature reflected by the standardized precipitation index (SPI) and the sensitivity of the PDSI to changes in evaporation demand caused by temperature fluctuations and trends. The nearest grid data of PDSI (118°45′E, 48°45′N, 1953–2005) (Dai et al., 2004) and SPEI (119°45′E, 47°45′N; 119°45′E, 48°15′N, 1953–2011) (Vicente-Serrano et al., 2010b) were abstracted for climate-growth response analyses.

2.2. Tree-ring data

Mongolian pine (*Pinus sylvestris* var. *mongolica*) is a dominant conifer species in this region. One or two cores were sampled from each living tree, and a total of 35 cores were collected from 28 Mongolian pines at site of SSQ (48°13′07.48″–48°13′19.93″N, 119°56′02.97″–119°56′15.80″E, 773 m a.s.l.) in August 2013 (Fig. 1). In the laboratory, all the ring-width samples were treated according to standard dendrochronological procedures (Cook and Kairiukstis, 1990; Fritts, 2001), and measured with a precision of 0.01 mm using LINTAB6 measuring device. The COFECHA program (Holmes, 1983) was applied to assess the quality of the cross-dating of tree-ring series. After removing several cores with poor correlations with the master sequence, the COFECHA results showed that average correlation coefficient between individual series and the master series was 0.618, mean sensitivity was 0.208 and absent rings rate was 0.073%. The ARSTAN program (Cook, 1985) was utilized to develop the final tree-ring chronology. Apart from two cores that were treated using the cubic smoothing spline with a 50-year window (about 2/3 of the series length), most series were standardized by negative exponential curves or linear regression curves. Finally, the standard chronology of SSQ (SSQstd) was developed by averaging the index values using a biweight robust mean. (Cook and Kairiukstis, 1990). To decrease the effects of changing sample depth through time, the variance of SSQstd was stabilized following the Rbar-weighted method (Osborn et al., 1997). Subsample signal strength (SSS) was applied to assess the reliable beginning year of the chronology, and a value greater than 0.85 was acceptable (Wigley et al., 1984). The high values of Running expressed population signal (EPS, the same criterion as SSS) and Running Rbar (moving correlations between all the series) also indicated the chronology signal strength through time (Wigley et al., 1984). The entire SSQstd was 234-year in length with a span of 1780–2013, and the reliable interval (SSS > 0.85) started in 1819 and corresponded to four cores from four trees.

2.3. Statistical methods

Correlation analyses were utilized to explore the relationships between ring-width growth and climate variables during their period of overlap. Monthly total precipitation, mean and max temperature, SPEI and PDSI from the previous August to current September were used in the analysis. Correlations between climate variables of various seasons and SSQstd were also identified. Linear regression model was employed to reconstruct mean February–July SPEI. Split-sample method (Meko and Graybill, 1995) and Pearson's correlation coefficient (r) (Cook and Kairiukstis, 1990), sign test (ST), reduction of error (RE), coefficient of efficiency (CE), and product mean (t) were applied to evaluate the skills of the regression model. Positive values of RE and CE both testing the shared variance between actual and estimated series suggest that the reconstruction owns acceptable capacity (Cook et al., 1994, 1999). Regional climate signals in the tree-ring data was assessed in a spatial correlation analyses with gridded CRU TS3.22 (Harris et al., 2014), CSIC SPEI (Vicente-Serrano et al., 2010b) and NCDC ERSSTv3 (Smith et al., 2008) using the KNMI Climate Explorer (van Oldenborgh and Burgers, 2005). Period analyses were conducted using wavelet software (Torrence and Compo, 1998). The mean February–July SPEI reconstruction was evaluated

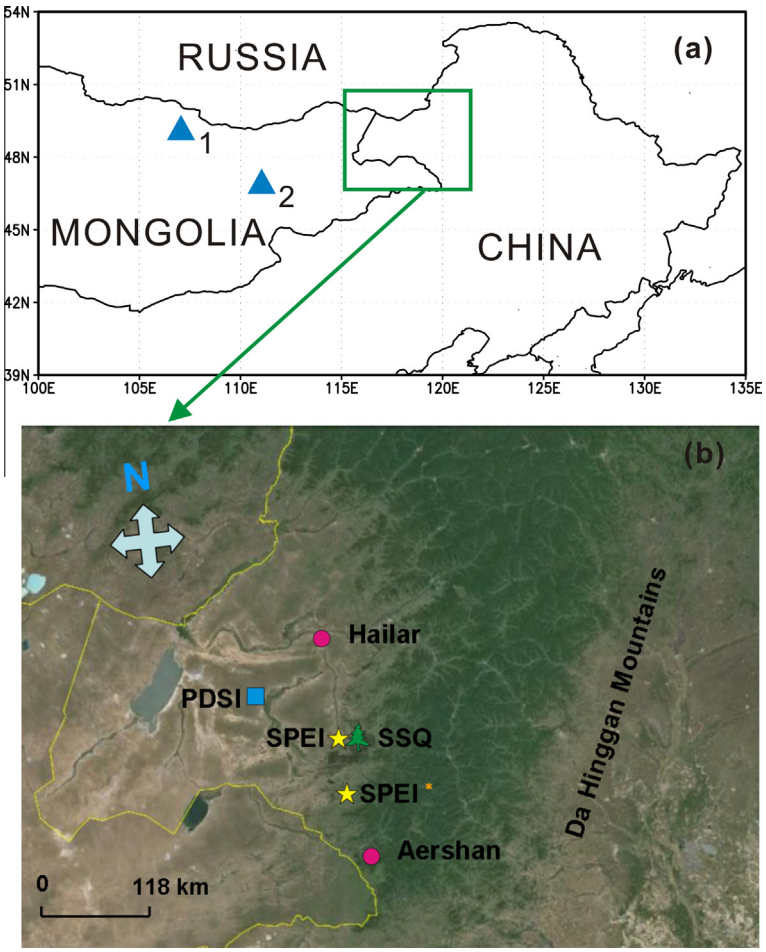

Fig. 1. (a) Map of the study area and positions of sites used in Fig. 7 (Pederson et al., 2013, triangle_1; Davi et al., 2013, triangle_2); (b) locations of the sampling site (SSQ) (green tree), Hailar and Aershan meteorological stations (red dots), PDSI grid (blue rectangle) and SPEI grid (yellow pentagon; the reconstructed one marked by *). (For interpretation of the references to color in this figure legend, the reader is referred to the web version of this article.)

for pluvial and drought characteristics, by using magnitude (sum of the departure values from the long-term median) and intensity (sum of the departure values from the median divided by the duration) of each events (three years or greater) through time (Biondi et al., 2002).

3. Results

3.1. Climate-growth response

The SSQstd was significantly and positively correlated with precipitation in previous August ($p < 0.05$), current May ($p < 0.1$) and July ($p < 0.05$), and negatively with mean temperature in previous September, current January, February, and June to September ($p < 0.05$) (Fig. 3). A similar response pattern was observed between tree-growth and maximum temperatures. The same patterns were revealed from the results of SSQstd with SPEI and PDSI data during the present growing year (Fig. 3). On the seasonal scale after combined several monthly variables, the highest correlation was found between SSQstd and the mean February–July SPEI ($r = 0.573$, $p < 0.0001$, $n = 59$, 1953–2011; 119°45′E, 47°45′N).

3.2. Reconstruction

Based on the distinct response relationships between tree growth of SSQstd and climate variables, the mean February–July SPEI was reconstructed utilizing a simple linear regression model, as follows: $Yi = 1.826 \times SSQstdi - 1.838$ ($p = 0.001$, Durbin–Watson value = 1.916), where Y*i* refers to the mean February–July SPEI, *i* indicates the current year. The model could explain 32.8% (31.7% after considering the loss of degrees of freedom) for the calibration period 1953–2011. The statistics in the verification and calibration indicated the model was reliable and steady (Table 1). Particularly, the most rigorous tests of RE and CE were positive for both verification periods verifying acceptable skills of our reconstruction (Cook and Kairiukstis, 1990; Fritts, 2001). The high values of Running EPS and Rbar also demonstrated the reliability of this drought reconstruction (Fig. 4). The observed and reconstructed series and their first difference matched each other quite well ($r = 0.573$, $p < 0.0001$; $r = 0.548$, $p < 0.0001$, respectively) (Fig. 4(a) and (b)). And both high and low frequencies variations of the reconstructed mean February–July $SPEI_{1month}$ (RECSPEI27) for 1819–2013 were shown in Fig. 4(c).

3.3. Features of RECSPEI27

The RECSPEI27 varied in a range from −0.742 to 1.12, with a mean of −0.04 and a standard deviation (SD) of 0.328 of the whole span. Extreme pluvial and drought episodes were defined as SPEI > 0.288 (mean + 1SD) and SPEI < −0.368 (mean−1SD), respectively. According to these criteria, 37 extremely dry years and 28 extremely wet years occurred in our reconstruction, accounting for 18.97% and 14.36% of the entire period, respectively

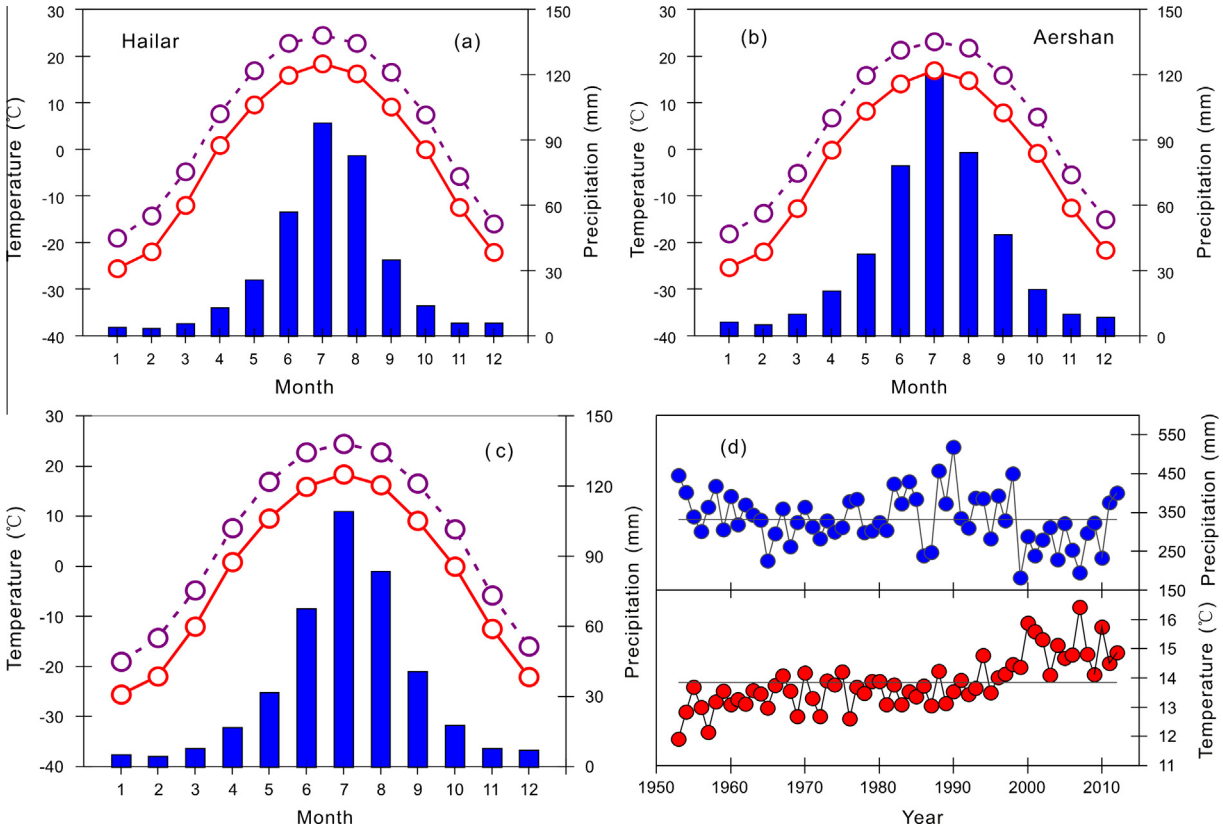

Fig. 2. Monthly sum of precipitation (filled bar), mean temperature (unfilled red dot) and mean max temperature (unfilled purple dot) of (a) Hailar and (b) Aershan meteorological stations; (c) the average value of both stations (1953–2012); (d) variations of the total precipitation of May–September and mean temperature of May–September of the average data of both stations (1953–2012). (For interpretation of the references to color in this figure legend, the reader is referred to the web version of this article.)

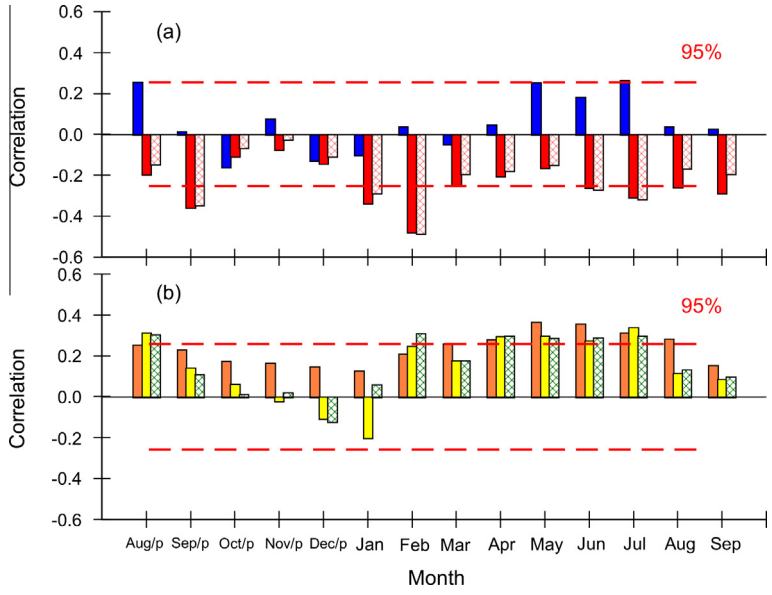

Fig. 3. Correlations between tree-ring standard chronology (SSQstd) and monthly climatic variables from the previous August to current September at the 95% confidence level (a) precipitation (blue bar), mean temperature (red bar) and max temperature (red cross bar), and (b) PDSI (brown bar, 118°45′E, 48°45′N, 1953–2005), SPEI (yellow bar, 119°45′E, 48°15′N; green cross bar 119°45′E, 47°45′N, 1953–2011). (For interpretation of the references to color in this figure legend, the reader is referred to the web version of this article.)

(Table S1). The magnitude and intensity of multi-year pluvial and dry events were shown in Table 2. Significant periods were found at years of 5.88 ($p < 0.1$), 6.93 ($p < 0.05$), 8.43 ($p < 0.1$), 9.70 ($p < 0.05$), 10.78 ($p < 0.05$), 13.86 ($p < 0.01$), 17.64 ($p < 0.05$), 32.33 ($p < 0.1$), 48.50 ($p < 0.1$) and 64.67 ($p < 0.1$) (Fig. 5(a)), and similar periods were also appeared in wavelet spectrum (Fig. 5(b)).

Table 1
Statistics of the split calibration and verification model for the mean February–July SPEI reconstruction.

Calibration					Verification						
Period	r	R^2	ST	t	Period	r	R^2	RE	CE	ST	t
1953–1982	0.453*	0.205	24+/5−*	3.391*	1983–2011	0.512*	0.262	0.539	0.198	19+/9−	5.522*
1983–2011	0.512*	0.262	19+/9−	5.522*	1953–1982	0.453*	0.205	0.455	0.122	24+/5−*	3.391*
1953–2011	0.573*	0.328	43+/15−*	7.595*							

RE refers to reduction error, CE indicates coefficient of efficiency, and ST means sign test at the high frequency, respectively.
* $p < 0.01$.

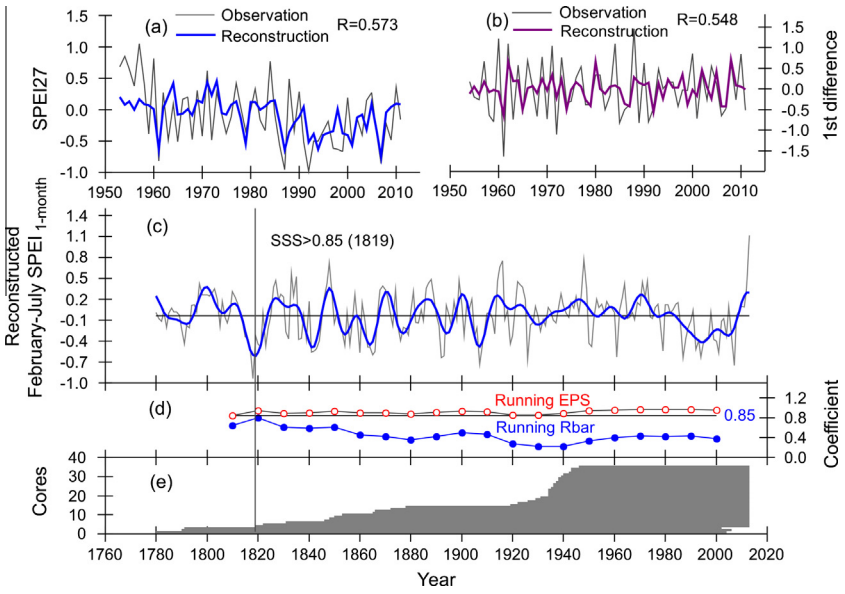

Fig. 4. Comparisons (a) between reconstructed and observed mean February–July SPEI during the span of 1953–2011, (b) between the first differences of mean February–July SPEI reconstruction and observation for 1953–2011, (c) variations of the reconstruction RECSPEI27 over the entire span of 1819–2013 for eastern Hulun Buir steppe (the bold line represents the 10-year low pass data and the horizontal line indicates the mean value of 1819–2013, (d) The running Rbar (based upon a 20-year window lagged 10 years) and the running expressed population signal (EPS) of SSQstd, the reliable portion of the chronology is determined by the SSS value >0.85, and (e) sample depth.

Table 2
Magnitude and intensity of dry and pluvial events three-year or more in duration for the reconstructed mean February–July SPEI.

Years	Duration	Magnitude	Intensity	Year	Duration	Magnitude	Intensity
1819–1821	3	−1.20	−0.40	1826–1830	5	1.63	0.33
1823–1825	3	−0.68	−0.23	1833–1835	3	1.40	0.47
1836–1839	4	−1.07	−0.27	1846–1849	4	1.72	0.43
1841–1845	5	−2.04	−0.41	1867–1872	6	1.38	0.23
1852–1854	3	−0.72	−0.24	1886–1890	5	1.62	0.32
1862–1866	5	−2.14	−0.43	1902–1904	3	0.47	0.16
1875–1879	5	−1.21	−0.24	1914–1916	3	1.93	0.64
1891–1893	3	−1.37	−0.46	1921–1925	5	1.61	0.32
1905–1909	5	−1.90	−0.38	1938–1941	4	0.53	0.13
1926–1928	3	−0.90	−0.30	1943–1949	7	1.94	0.28
1930–1933	4	−0.50	−0.13	1953–1960	8	0.91	0.11
1950–1952	3	−0.93	−0.31	1962–1964	3	0.73	0.24
1986–1990	5	−1.43	−0.29	1969–1973	5	1.49	0.30
1992–1997	6	−2.53	−0.42	1980–1985	6	0.69	0.12
1999–2004	6	−1.75	−0.29	2009–2013	5	1.80	0.36
2006–2008	3	−1.06	−0.35				

Multi-annual cycles existed over the entire span, but strong cycles on decadal scales only existed before 1910s.

4. Discussions

4.1. Climate-growth relationships

The positive response of tree growth to precipitation and negative to temperature suggests that drought stress is the major limiting factor for the *P. sylvestris* var. *mongolica* radial growth across the Hulun Buir steppe (Fig. 3(a)). This is further supported by the significant relationship between the SSQstd chronology and the PDSI and SPEI (Fig. 3(b)). Similar patterns have been found in arid and semiarid areas of northern China (Bao et al., 2015; Cai et al., 2010; Fang et al., 2012; Song and Liu, 2011). The fact that the tree-ring widths are more responsive to temperature than to precipitation during the growing season from April to September suggests that tree growth is dominated by temperature-induced

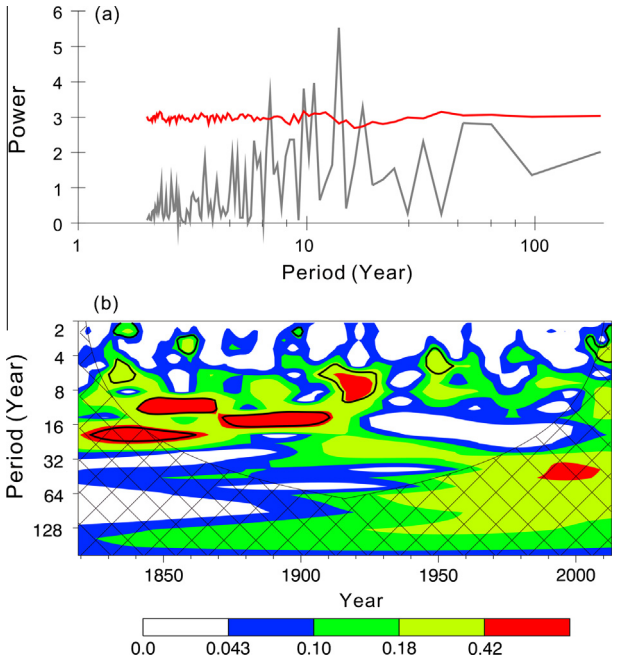

Fig. 5. Results of (a) power spectrum, (b) wavelet (Morlet 6; Torrence and Compo, 1998) analyses for reconstructed mean February–July SPEI for the period 1819–2013. The 95% confidence interval for peaks in the power spectrum is indicated by the red line. The cone of influence in the wavelet analysis is indicated by the cross line. Dark areas fixed by black contour (the 90% confidence level, using a red-noise (autoregressive lag 1) background spectrum) marked regions of significant power at corresponding timescales. (For interpretation of the references to color in this figure legend, the reader is referred to the web version of this article.)

drought stress (e.g. Fang et al., 2012; Liang et al., 2007). The increasing trend in mean May–September temperature also supports this point (Fig. 2(d)). Recent research obtained from North China at a location south of our study area has found that spring and summer PDSI was strongly governed by temperature than by precipitation (Cai et al., 2015). It should be noted that negative relationship between tree-ring width and temperature in January and February may reflect nutrient depletion caused by the respiration of trees (Wang et al., 2005). They found that low temperature in winter and early spring could effectively inhibit the respiration of *Larix gmelinii* in Mohe, a location about 200 km north of our study area, and accumulated nutrients in the trees could be utilized in the formation of radial cells during the current growing period.

4.2. Regional comparison and teleconnection

The most extreme hydroclimatic events in the reconstruction events seem to have been large in spatial extent. Extremely dry years of 2007 (<2SD), 1907 (<2SD), 1892 (<1SD), 1961 (<1SD), 1987 (<1SD) and 1951 (<1SD) were present in existing tree-ring moisture reconstructions adjacent to the study site (Bao et al., 2015; Chen et al., 2012). For instance, the severe drought in 2007 (<2SD) and 1951 (<1SD) affected most parts of central and eastern Mongolian Plateau (see Fig. 6(b) in Bao et al. (2015)). The year 1987 (<1SD) was recorded by the lowest runoff of hydrological stations such as Yiminmuchang, Bahou, Cuogang and Yakeshi stations in the Hulun Buir region (Duan et al., 2010). It was reported that the total precipitation from spring to summer (late June) of Xinbaerhuyou Banner Meteorologic station, southern Hulun Buir steppe, was 13.9 mm during the harsh drought in 1961 (<1SD) (http://www.nmg.xinhuanet.com/zt/2011-07/03/content_23212316.htm).

On decadal scales (after 10-year low pass filtered), significant fluctuations with a large magnitude appeared during 1820s–1910s in RECSPEI27, and severe drought interval in late 1970s–2000s followed the relative moisture period in 1930s–early 1970s (Fig. 4(c)). Similar variations also existed in the annual precipitation reconstruction from Honghuaerji, a location close to our study site (see Fig. 4(b) in Chen et al. (2012)), our drought reconstruction RECSPEI27 could represent a regional-scale moisture signal in a large area. This feature was also confirmed by spatial correlation analyses between RECSPEI27 and gridded instrumental climate data, including temperature, precipitation and SPEI (Fig. 6). The area of highest correlation occurred in and around the eastern Mongolian Plateau (Fig. 6), even stretching to the central Mongolia Plateau according to the temperature and SPEI field (Fig. 6 (a) and (c)). Therefore, two available moisture reconstructions based on tree-ring width were used to explore hydroclimatic variations in the central and eastern parts of the Mongolia Plateau through time. The first sequence is an August–July streamflow reconstruction of the Kherlen River in northeastern Mongolia, a location approximately 800 km west of our study area (Davi et al., 2013). The second one, from a location approximately 1000 km northwest of our study area, is a reconstruction of the May–September streamflow of the Yeruu River in northern Mongolia (Pederson et al., 2013). Common drought periods in the late 1830s–early 1840s, the late 1890s–1910s, 1920s–1930s and 1950s occurred in all three records on a bidecadal scale (Fig. 7), which suggests that our reconstruction captures extra-basin-scale events (Davi et al., 2013), and thereby reflects a large-scale regional hydroclimatic signal in and around the eastern Mongolian Plateau. Notably, the apparent severe drought conditions since the late 1970s in our RECSPEI27 was not evident in the streamflow reconstructions from the Kherlen River (Davi et al., 2013) and the Yeruu River (Pederson et al., 2013). This might partly be explained by the weakening influence of the East Asian summer monsoon on tree growth in our study site. Previous studies have found that the intensity of the East Asian summer monsoon weakened from the late 1970s (Cook et al., 2010; Wang, 2001; Zhang et al., 2008), further led to great moisture supply deficient (such as precipitation) in North China (Ding et al., 2008) and the eastern Mongolian Plateau including our study area and its vicinity (Huang et al., 2013). The significant correlation between RECSPEI27 and East Asian summer monsoon index (Guo, 1983; Guo et al., 2004) ($r = 0.300$, $p = 0.034$, $n = 50$, 1951–2000; $r = 0.276$, $p = 0.013$, $n = 81$, 1920–2000) confirmed the decreasing moisture interval science the late 1970s in our drought reconstruction associated with the weakening East Asian summer monsoon.

Significant cycles on multi-annual and decadal scales in the RECSPEI27 reconstruction implied that other factors may influence drought conditions in this area (Fig. 4). Significant peaks of 17.64 ($p < 0.05$), 32.33 ($p < 0.1$) and 48.50 ($p < 0.1$), 64.67 ($p < 0.1$) years responding to the periods of ~20–30 and ~50–70 years of the Pacific Decadal Oscillation (PDO) (Gedalof et al., 2002; Minobe, 1999) and significantly negative (positive) correlation with the SST in the eastern Pacific Ocean along the North America west coast (Central-North Pacific Ocean) (Fig. 8) indicated the RECSPEI27 variability could be modulated by the PDO. The relationship between the PDO and the summer precipitation in eastern China has been explored (e.g. Gong and He, 2002; Shen et al., 2006). The PDO could modulate the strength of the summer monsoon and the position of the subtropical high, consequently alter summer precipitation over eastern China (Gong and He, 2002). In the PDO warm phases, the summer monsoon became weak and the strong subtropical high associated with its position locating far to the south and west, which caused anomalous dry periods in both North and South China, and wet periods in the middle and lower Yangtze River Valley. The opposite moisture variations occurred in the PDO cold phases (Gong and He, 2002; Shen et al., 2006). The annual PDO index with a period from 1470 to 2000 AD was reconstructed based on a data set of drought/flood index (a proxy of summer

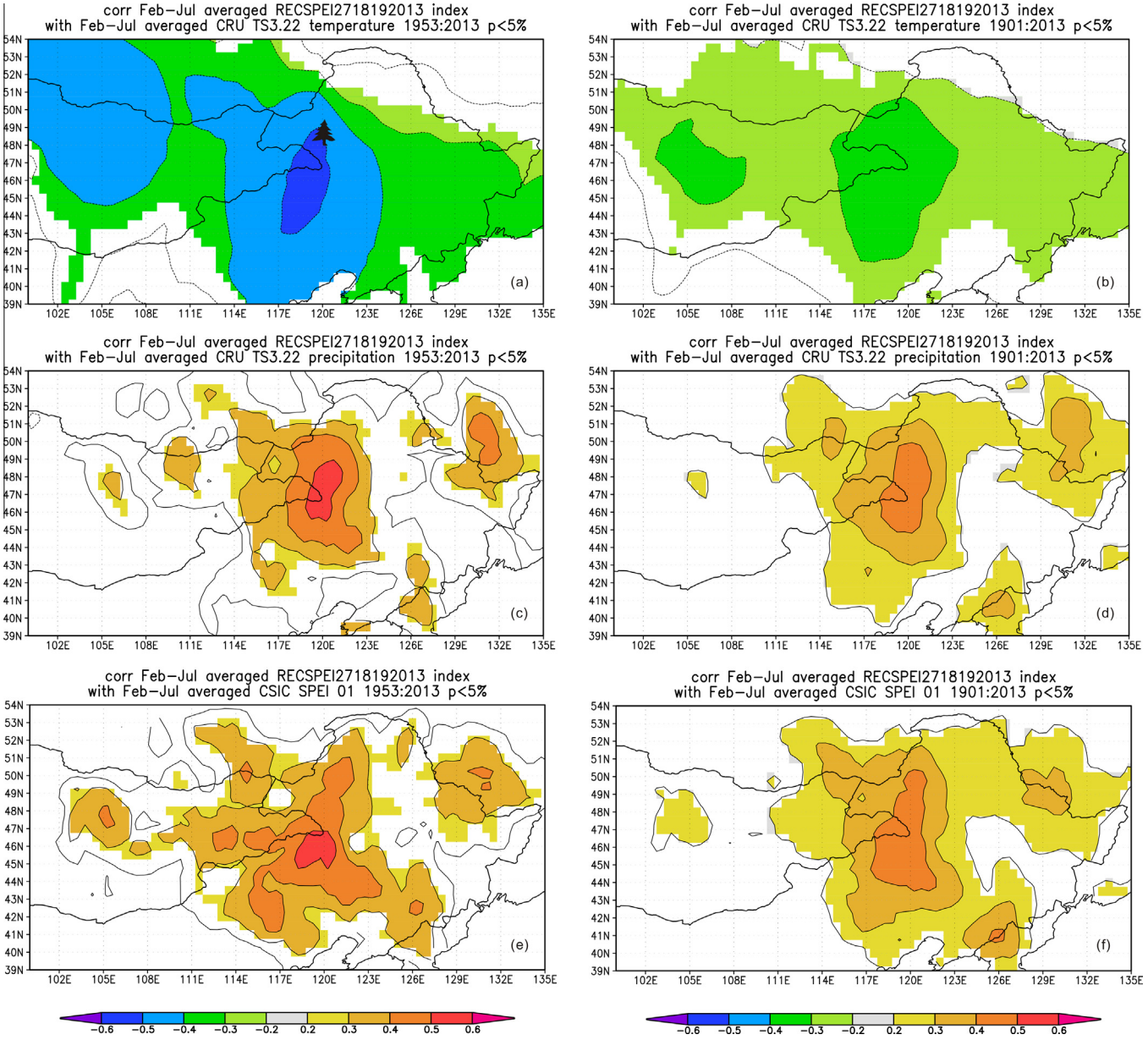

Fig. 6. Spatial correlation fields of reconstructed mean February–July SPEI with (a) mean temperature and (c) total precipitation of February–July of CRU TS3.22 grid dataset during 1953–2013 (Harris et al., 2014), (e) the average February–July SPEI01 dataset (Vicente-Serrano et al., 2010b) during 1953–2013; (b), (d) and (f) for the period of 1901–2013. The correlation coefficient value of 95% confidence level is 0.252 for 1953–2013 (0.185 for 1901–2013). The sampling site (SSQ) marked by black tree.

rainfall) obtained from Chinese historical documents in eastern China. And the reconstruction implied that the PDO is a robust feature of North Pacific climate variability throughout the whole period (Shen et al., 2006). Recently, Qian and Zhou (2014) have demonstrated the close connection between PDSI in North China and the PDO index during the period of 1900–2010. Composite difference results indicated that similar wave train of the Pacific–Japan/East Asia–Pacific (PJ/EAP) may respond to the warm SST anomalies in the tropical Indo-Pacific Ocean associated with the PDO, and spread from the tropical western Pacific to North China along the East Asian coast. In the warm PDO phase, North China tends to experience more drought condition because of the strong influence of anomalous high pressure and anticyclone system in the mid-lower troposphere over this region. The possible mechanism of the PDO affecting the South Asian monsoon rainfall is through the seasonal footprinting of SST (Vimont et al., 2001, 2003) from the North Pacific to the subtropical Pacific and further the Walker and Hadley circulations suggested by Krishnamurthy and Krishnamurthy (2013). Significant correlation between RECSPEI27 and the PDO index (Felis et al., 2010) ($r = -0.222$, $p = 0.014$, $n = 122$, 1873–1994) and their 11-year sliding correlation (not shown) confirmed the relationship of drought variations in the eastern Mongolian Plateau and remote ocean area. The influence of the PDO on tree growth in Asia had been investigated based on tree-ring material (e.g. Bao et al., 2015; Chen et al., 2012; D'Arrigo and Wilson, 2006).

Peaks of 5.88 ($p < 0.1$) and 6.93 ($p < 0.05$) years within the 2–8-year range of the El Niño-Southern Oscillation (ENSO) (Allan et al., 1996; Sun and Wang, 2007) suggested possible links to the eastern tropical Pacific Ocean. The Multivariate ENSO Index (MEI), based on six main variables over the tropical Pacific, is considered to be more appropriate than other indices for the overall monitoring of the ENSO.ENSO than other series (Wolter and Timlin, 2011). Our mean February–July SPEI reconstruction negatively correlated with

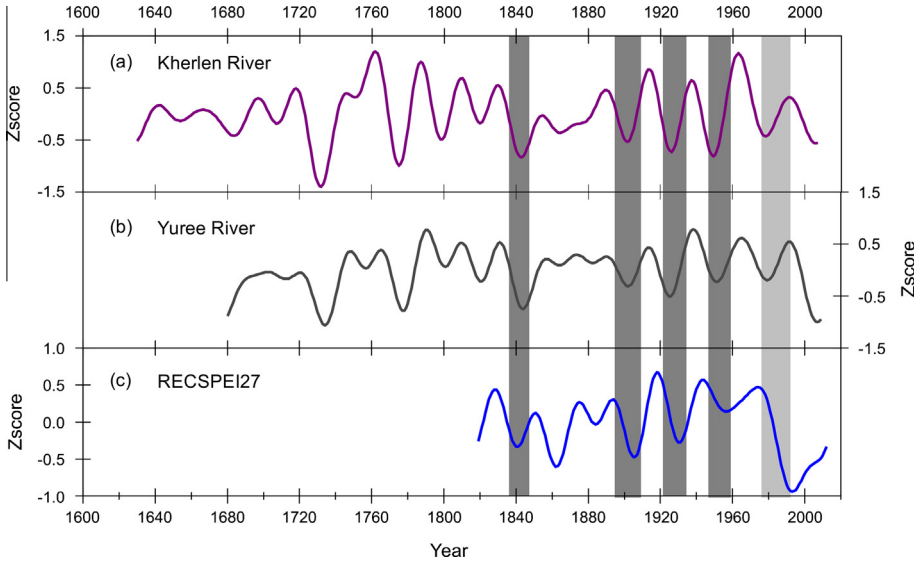

Fig. 7. Comparisons of (a) August–July streamflow reconstruction of the Kherlen River in northeastern Mongolia (Davi et al., 2013), (b) May–September streamflow reconstruction of the Yeruu River in northern Mongolia (Pederson et al., 2013) and (c) the mean February–July SPEI reconstruction for eastern Hulun Buir steppe (in this study). All the records have been standardized as Zscore. The bold line represents the 20-year low pass data. The dark shaded areas represent common drought intervals and light shaded area refers to the different interval.

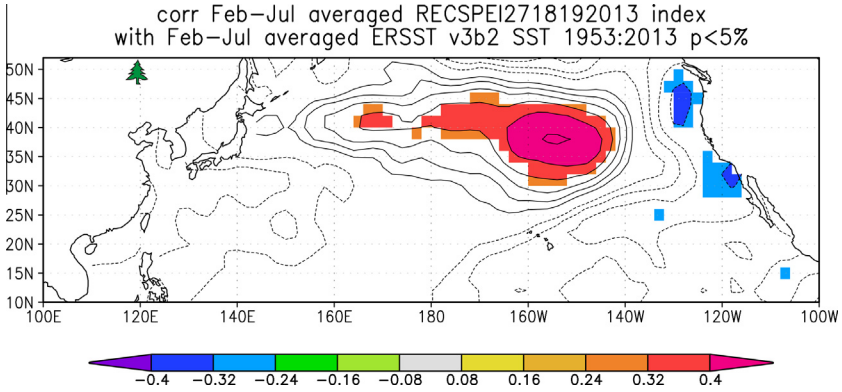

Fig. 8. Spatial correlation between reconstructed mean February–July SPEI for eastern Hulun Buir steppe and the sea surface temperature of NCDC ERSSTv3 (Smith et al., 2008) during the period 1953–2013. The correlation coefficient value of 95% confidence level is 0.252 for 1953–2013. The sampling site (SSQ) marked by green tree. (For interpretation of the references to color in this figure legend, the reader is referred to the web version of this article.)

MEI in June (−0.211, $p < 0.1$, 1950–2013) and August (−0.231, $p < 0.1$), as well as May–August (−0.218, $p < 0.1$). Low correlation coefficients may imply weak connection between tree growth and remote tropical Pacific. However, significantly negative correlations were found between tree rings in Honghuaerji and MEI in April–July (Chen et al., 2012). The similarly negative responses were also confirmed by spatial correlations inferred from Mongolian Pines and central-eastern parts of the Pacific (see Fig. S1 in Bao et al. (2015)). It may be the case as suggested by Cook et al. (1998) and George (2014), i.e. many records within a tree-ring network do not strongly respond to a specific climate mode does not mean that forcing has no effect on these records. It is possible that these records are more sensitive to a particular remote forcing than other records from the same region or species.

Previous studies have reported that ENSO may be an important factor influencing precipitation in and around northern China through modulating the strength of the Asian summer monsoon (Lu, 2005; Xu et al., 2010). For the enhanced SST in the eastern equatorial Pacific Ocean in the El Niño phase and the temperature gradient between tropical and subtropical ocean, the eastern subtropical Pacific becomes warmer in summer. That induces a zonal anomalous circulation over the subtropical–tropical Pacific Ocean, further results in a strengthened western Pacific subtropical high (WPSH). Associated with a westward shift of the subtropical high, moisture in the semi-arid region of North China could be reduced for the weakening influence of the Indian summer monsoon on its northerly marginal zone (Fu and Li, 1978; Li et al., 1979). The intensification of the WPSH related to the warming in the eastern tropical Pacific Ocean has been confirmed by an idealized model experiment (Yu et al., 2014). Significantly negative correlation between our reconstruction and the SSTs across the eastern subtropical Pacific may support the connection between our reconstruction and remote climate forcing (Fig. S1). Hence, the harsh drought in 1926 (<1SD) seen in RECSPEI27 (Table 2) is likely caused by the strong El Niño events in 1925 and 1926 (Quinn and Neal, 1992).

5. Conclusions

A mean February–July standardized precipitation evapotranspiration index reconstruction has been developed utilizing a tree-ring width chronology of *P. sylvestris* var. *mongolica* from the

eastern Hulun Buir steppe, a marginal area located in the eastern part of the Mongolian Plateau. Regional hydroclimatic characteristics are disclosed by the common fluctuations of drought and pluvial durations in other tree-ring-based reconstructions and ours. Serious drought intervals since the late 1970s occurred in this reconstruction may respond to the influence of the weakening East Asian summer monsoon on tree growth in our study area. Teleconnections between the reconstruction and SSTs in the Pacific Ocean confirm the linkages of moisture variations in the eastern Mongolian Plateau and remote oceans. To deeply understand the spatial and temporal features of drought variations in such a large climate-sensitive area, more tree-ring investigations should be conducted and more parameters such as stable isotopes and density should be involved. Tree-ring stable oxygen isotope studies have been conducted in North China, a limiting area of Asian summer monsoon, which demonstrated the teleconnection between regional precipitation and remote oceans (Li et al., 2011, 2015). And the tree-ring density of Mongolian pines has been studied in Mohe, a location approximately 200 km north of our study area, which revealed more valuable signals comparing to ring-width series (Wang et al., 2005). Therefore, it will be helpful to explore the relationship between regional hydroclimatology and large scale climate forcing based on a multi-proxy dendroclimatology approach in the future, such as in eastern Hulun Buir steppe, Mongolian Plateau.

Acknowledgments

The authors thank Mrs. Xiting Liu and Miss Muxin Bao for their great help during the filed work. This work was supported by the National Natural Science Foundation of China (41301101), Natural Science Basic Research Plan in Shaanxi Province of China (Program No. 2014JQ5192), the State Key Laboratory of Loess and Quaternary Geology Foundation (SKLLQG1302), the Chinese Academy of Sciences (KZCX2-YW-Q1-01 and KZZD-EW-04), the One-hundred Talents Program of the Chinese Academy of Sciences, and National Basic Research Program of China (2013CB955903).

Appendix A. Supplementary material

Supplementary data associated with this article can be found, in the online version, at http://dx.doi.org/10.1016/j.jseaes.2015.10.009.

References

Allan, R.J., Lindesay, J.A., Parker, D.E., 1996. El Niño Southern Oscillation and Climatic Variability. CSIRO Publishing, Australia.
Bao, G., 2015. Mongolian pines (*Pinus sylvestris* var. *mongolica*) in the Hulun Buir steppe, China, respond to climate in adjustment to the local water supply. Int. J. Biometeorol. 59, 1–10.
Bao, G., Liu, Y., Liu, N., 2012. A tree-ring-based reconstruction of the Yimin River annual runoff in the Hulun Buir region, Inner Mongolia, for the past 135 years. Chin. Sci. Bull. 57 (36), 4765–4775.
Bao, G., Liu, Y., Liu, N., Linderholm, H.W., 2015. Drought variability in eastern Mongolian Plateau and its linkages to the large-scale climate forcing. Clim. Dyn. 44 (3–4), 717–733.
Batima, P., 2006. Potential impacts of climate change and vulnerability and adaptation assessment for grassland ecosystem and livestock sector in Mongolia. Final Report: Observed climate change in Mongolia, AIACC. Project AS06. Institute of Meteorology and Hydrology, Ulaanbaatar, Mongolia.
Biondi, F., Kozubowski, T.J., Panorska, A.K., 2002. Stochastic modeling of regime shifts. Climate Res. 23 (1), 23–30.
Cai, Q., Liu, Y., Liu, H., Ren, J., 2015. Reconstruction of drought variability in North China and its association with sea surface temperature in the joining area of Asia and Indian–Pacific Ocean. Palaeogeogr. Palaeoclimatol. Palaeoecol. 417, 554–560.
Cai, Q.F., Liu, Y., Bao, G., Lei, Y., Sun, B., 2010. Tree-ring-based May–July mean temperature history for Lüliang Mountains, China, since 1836. Chin. Sci. Bull. 55, 3008–3014.
Chen, Z.J., Zhang, X.L., Cui, M.X., He, X.Y., Ding, W.H., Peng, J.J., 2012. Tree-ring based precipitation reconstruction for the forest-steppe ecotone in northern Inner Mongolia, China and its linkages to the Pacific Ocean variability. Global Planet. Change 86–87, 45–56.
Chinese Academy of Sciences (Compilatory Commission of Physical Geography of China), 1984. Physical Geography of China: Climate. Science Press, Beijing (in Chinese).
Cook, E., Kairiukstis, L., 1990. Methods of Dendrochronology: Applications in the Environmental Science. Kluwer, Dordrecht.
Cook, E.R., 1985. A Time Series Analysis Approach to Tree Ring Standardization. PhD. The University of Arizona, Tucson.
Cook, E.R., Briffa, K.R., Jones, P.D., 1994. Spatial regression methods in dendroclimatology: a review and comparison of two techniques. Int. J. Climatol. 14, 379–402.
Cook, E.R., D'Arrigo, R.D., Briffa, K.R., 1998. A reconstruction of the North Atlantic Oscillation using tree-ring chronologies from North America and Europe. Holocene 8, 9–17.
Cook, E.R., Meko, D.M., Stahle, D.W., Cleaveland, M.K., 1999. Drought reconstructions for the continental United States. J. Clim. 12, 1145–1162.
Cook, E.R., Woodhouse, C.A., Eakin, C.M., Meko, D.M., Stahle, D.W., 2004. Long-term aridity changes in the western United States. Science 306 (5698), 1015–1018.
Cook, E.R., Anchukaitis, K.J., Buckley, B.M., D'Arrigo, R.D., Jacoby, G.C., Wright, W.E., 2010. Asian monsoon failure and megadrought during the last millennium. Science 328, 486–489.
Dai, A., 2011. Drought under global warming: a review. Wiley Interdiscipl. Rev.: Clim. Change 2 (1), 45–65.
Dai, A.G., Trenberth, K.E., Qian, T., 2004. A global dataset of palmer drought severity index for 1870–2002: relationship with soil moisture and effects of surface warming. J. Hydrometeorol. 5, 1117–1130.
D'Arrigo, R., Jacoby, G., Frank, D., Pederson, N., Cook, E., Buckley, B., Nachin, B., Mijiddorj, R., Dugarjav, C., 2001. 1738 years of Mongolian temperature variability inferred from a tree-ring width chronology of Siberian pine. Geophys. Res. Lett. 28, 543–546.
D'Arrigo, R., Jacoby, G., Pederson, N., Frank, D., Buckley, B., Nachin, B., Mijiddorj, R., Dugarjav, C., 2000. Mongolian tree-rings, temperature sensitivity and reconstructions of Northern Hemisphere temperature. Holocene 10, 669–672.
D'Arrigo, R., Wilson, R., 2006. On the Asian expression of the PDO. Int. J. Climatol. 26 (12), 1607–1617.
Davi, N., Jacoby, G., D'Arrigo, R., Baatarbileg, N., Li, J., Curtis, A., 2009. A tree-ring based drought index reconstruction for far western Mongolia: 1565–2004. Int. J. Climatol. 29, 1508–1514.
Davi, N., Jacoby, G., Fang, K., Li, J., D'Arrigo, R., Baatarbileg, N., Robinson, D., 2010. Reconstructing drought variability for Mongolia based on a large-scale tree ring network: 1520–1993. J. Geophys. Res. 115, D22103. http://dx.doi.org/10.1029/2010JD013907.
Davi, N.K., Jacoby, G.C., Curtis, A.E., Baatarbileg, N., 2006. Extension of drought records for central Asia using tree rings: West-central Mongolia. J. Clim. 19, 288–299.
Davi, N.K., Pederson, N., Leland, C., Nachin, B., Suran, B., Jacoby, G.C., 2013. Is eastern Mongolia drying? A long-term perspective of a multidecadal trend. Water Resour. Res. 49, 151–158.
Ding, Y.H., Wang, Z.Y., Sun, Y., 2008. Inter-decadal variation of the summer precipitation in East China and its association with decreasing Asian summer monsoon. Part I: Observed evidences. Int. J. Climatol. 28, 1139–1161.
Duan, L.M., Liu, T.X., Wang, X.X., Luo, Y.Y., Wu, L., 2010. Development of a regional regression model for estimating annual runoff in the Hailar River Basin of China. J. Water Resour. Prot. 2, 934–943.
Fang, K., Gou, X., Chen, F., Frank, D., Liu, C., Li, J., Kazmer, M., 2012. Precipitation variability during the past 400 years in the Xiaolong Mountain (central China) inferred from tree rings. Clim. Dyn. 39, 1697–1707.
Felis, T., Suzuki, A., Kuhnert, H., Rimbu, N., Kawahata, H., 2010. Pacific Decadal Oscillation documented in a coral record of North Pacific winter temperature since 1873. Geophys. Res. Lett. 37, L14605. http://dx.doi.org/10.1029/2010GL043572.
Fritts, H.C., 2001. Tree Rings and Climate. Blackburn Press, Caldwell, New Jersey.
Fu, C., Li, K., 1978. The Effects of Tropical Ocean on the Western Pacific Subtropical High. Oceanic Selections, No. 2. Ocean Press, pp. 16–21.
Gedalof, Z., Mantua, N.J., Peterson, D.L., 2002. A multi-century perspective of variability in the Pacific Decadal Oscillation: new insights from tree rings and coral. Geophys. Res. Lett. 29 (24), 2204. http://dx.doi.org/10.1029/2002GL015824.
George, S.S., 2014. An overview of tree-ring width records across the Northern Hemisphere. Quaternary Sci. Rev. 95, 132–150.
Gong, D., He, X., 2002. Interdacadal change in western Pacific subtropical high and climatic effects. Acta Geogr. Sinica 57, 185–193.
Guo, Q.Y., 1983. The summer monsoon intensity index in East Asia and its variation. Acta Geogr. Sinica 38 (3), 207–217.
Guo, Q.Y., Cai, J.N., Shao, X.M., Sha, W.Y., 2004. Studies on the variations of East-Asian Summer Monsoon during AD 1873–2000. Chin. J. Atmos. Sci. 28 (2), 206–215.
Harris, I., Jones, P.D., Osborn, T.J., Lister, D.H., 2014. Updated high-resolution grids of monthly climatic observations – the CRU TS3. 10 Dataset. Int. J. Climatol. 34 (3), 623–642.
Holmes, R.L., 1983. Computer-assisted quality control in tree-ring dating and measurement. Tree Ring Bull. 43, 69–78.
Huang, W., Chen, F.H., Feng, S., Chen, J.H., Zhang, X.J., 2013. Interannual precipitation variations in the mid-latitude Asia and their association with large-scale atmospheric circulation. Chin. Sci. Bull. 58 (32), 3962–3968.

Krishnamurthy, L., Krishnamurthy, V., 2013. Influence of PDO on South Asian monsoon and monsoon-ENSO relation. Clim. Dyn. http://dx.doi.org/10.1007/s00382-013-1856-z.
Li, J., Cook, E.R., D'arrigo, R., Chen, F., Gou, X., 2009. Moisture variability across China and Mongolia: 1951–2005. Clim. Dyn. 32 (7–8), 1173–1186.
Li, K.R., Chen, Y.S., Liu, J.F., Lan, R.H., 1979. Some facts about the effect of the meridional difference of SST anomalies of north Pacific on the subtropical high. Sci. Atmos. Sinica 3, 150–157.
Li, Q., Nakatsuka, T., Kawamura, K., Liu, Y., Song, H., 2011. Hydroclimate variability in the North China Plain and its link with El Niño-Southern Oscillation since 1784 AD: insights from tree-ring cellulose $\delta^{18}O$. J. Geophys. Res. Atmos. 116, D22106. http://dx.doi.org/10.1029/2011JD015987.
Li, Q., Liu, Y., Nakatsuka, T., Song, H., McCarroll, D., Yang, Y., Qi, J., 2015. The 225-year precipitation variability inferred from tree-ring records in Shanxi Province, the North China, and its teleconnection with Indian summer monsoon. Global Planet. Change 132, 11–19.
Liang, E.Y., Shao, X.M., Liu, H.Y., Eckstein, D., 2007. Tree-ring based PDSI reconstruction since AD 1842 in the Ortindag Sand Land, east Inner Mongolia. Chin. Sci. Bull. 52, 2715–2721.
Liu, Y., Bao, G., Song, H.M., Cai, Q.F., Sun, J.Y., 2009. Precipitation reconstruction from Hailar pine (*Pinus sylvestris* var. mongolica) tree rings in the Hailar region, Inner Mongolia, China back to 1865 AD. Palaeogeogr. Palaeoclimatol. Palaeoecol. 282, 81–87.
Liu, Y., Wang, Y., Li, Q., Song, H., Zhang, Y., Yuan, Z., Wang, Z., 2014. A tree-ring-based June–September mean relative humidity reconstruction since 1837 from the Yiwulü Mountain region, China. Int. J. Climatol. http://dx.doi.org/10.1002/joc.4057.
Lu, R., 2005. Interannual variation of North China rainfall in rainy season and SSTs in the quatorial eastern Pacific. Chin. Sci. Bull. 50, 2069–2073.
Meko, D.M., Graybill, D.A., 1995. Tree-ring reconstruction of upper Gila River discharge. J. Am. Water Resour. Assoc. 31, 605–616.
Minobe, S., 1999. Resonance in bidecadal and pentadecadal climate oscillations over the North Pacific: role in climatic regime shifts. Geophys. Res. Lett. 26 (7), 855–858.
Osborn, T.J., Briffa, K.B., Jones, P.D., 1997. Adjusting variance for sample size in tree-ring chronologies and other regional mean timeseries. Dendrochronologia 15, 89–99.
Pederson, N., Jacoby, G.C., D'Arrigo, R.D., Cook, E.R., Buckley, B.M., Dugarjav, C., Mijiddorj, R., 2001. Hydrometeorological reconstructions for Northeastern Mongolia derived from tree rings: 1651–1995. J. Clim. 14, 872–881.
Pederson, N., Lealand, C., Nachin, B., Hessl, A.E., Bell, A.R., Martin-Benito, D., Saladyga, T., Suran, B., Brown, P.M., Davi, N., 2013. Three centuries of shifting hydroclimatic regimes across the Mongolian Breadbasket. Agric. For. Meteorol. 178–179, 10–20.
Qian, C., Zhou, T.J., 2014. Multidecadal variability of North China aridity and its relationship to PDO during 1900–2010. J. Clim. 27, 1210–1222.
Quinn, W.H., Neal, V.T., 1992. The historical record of El Nino events. In: Bradley, R. S., Jones, P.D. (Eds.), Climate since 1500 AD. Routledge, London, pp. 623–648.
Shen, C., Wang, W.C., Gong, W., Hao, Z., 2006. A Pacific Decadal Oscillation record since 1470 AD reconstructed from proxy data of summer rainfall over eastern China. Geophys. Res. Lett. 33, L03702. http://dx.doi.org/10.1029/2005GL024804.
Shen, J.G., 2008. Meteorological Disasters Dictionary of China: Inner Mongolia. Meteorological Press, Beijing (in Chinese).
Smith, T.M., Reynolds, R.W., Peterson, T.C., Lawrimore, J., 2008. Improvements to NOAA's historical merged land–ocean surface temperature analysis (1880–2006). J. Clim. 21, 2283–2296.
Song, H., Liu, Y., 2011. PDSI variations at Kongtong Mountain, China, inferred from a 283-year *Pinus tabulaeformis* ring width chronology. J. Geophys. Res. 116, D22111. http://dx.doi.org/10.1029/2011JD016220.
Sun, M., Wang, H., 2007. Relationship and its instability of ENSO–Chinese variations in droughts and wet spells. Sci. China, Ser. D Earth Sci. 50, 145–152.
Torrence, C., Compo, G.P., 1998. A practical guide to wavelet analysis. Bull. Am. Meteorol. Soc. 79, 61–78.
Trenberth, K., Overpeck, J., Solomon, S., 2004. Exploring drought and its implications for the future. Eos, Trans. Am. Geophys. Union 85 (3), 27–29.
Van Oldenborgh, G.J., Burgers, G., 2005. Searching for decadal variations in ENSO precipitation teleconnections. Geophys. Res. Lett. 32, L15701. http://dx.doi.org/10.1029/2005GL023110.
Vicente-Serrano, S.M., Beguería, S., López-Moreno, J.I., 2010a. A multiscalar drought index sensitive to global warming: the standardized precipitation evapotranspiration index. J. Clim. 23 (7), 1696–1718.
Vicente-Serrano, S.M., Beguería, S., López-Moreno, J.I., Angulo, M., El Kenawy, A., 2010b. A new global 0.5°gridded dataset (1901–2006) of a multiscalar drought index: comparison with current drought index datasets based on the Palmer Drought Severity Index. J. Hydrometeorol. 11 (4), 1033–1043.
Vimont, D.J., Battisti, D.S., Hirst, A.C., 2001. Footprinting: a seasonal connection between the tropics and midlatitudes. Geophys. Res. Lett. 28, 3923–3926.
Vimont, D.J., Battisti, D.S., Hirst, A.C., 2003. The seasonal footprinting mechanism in the CSIRO general circulation models. J. Clim. 16, 2653–2667.
Wang, H.J., 2001. The weakening of the Asian monsoon circulation after the end of 1970's. Adv. Atmos. Sci. 18, 376–386.
Wang, L.L., Shao, X.M., Huang, L., Liang, E.Y., 2005. Tree-ring characteristics of *Larix gmelinii* and *Pinus sylvestris* Var. Mongolia and their response to climate in Mohe, China. Acta Phytoecol. Sinica 29, 380–385 (in Chinese).
Wang, X.M., Zhang, C.X., Hasi, E., Dong, Z.B., 2010. Has the Three Norths Forest Shelterbelt Program solved the desertification and dust storm problems in arid and semiarid China? J. Arid Environ. 74, 13–22.
Wigley, T.M.L., Briffa, K.R., Jones, P.D., 1984. Average value of correlated time series, with applications in dendroclimatology and hydrometeorology. J. Clim. Appl. Meteorol. 23, 201–234.
Wilhite, D.A., 2000. Drought as a natural hazard: concepts and definitions. In: Wilhite, D.A. (Ed.), Droughts: Global Assessment. Routledge, London, pp. 3–18.
Wolter, K., Timlin, M.S., 2011. El Niño/Southern Oscillation behaviour since 1871 as diagnosed in an extended multivariate ENSO index (MEI. ext). Int. J. Climatol. 31 (7), 1074–1087.
Xu, H., Hong, Y., Hong, B., Zhu, Y., Wang, Y., 2010. Influence of ENSO on multi-annual temperature variations at Hongyuan, NE Qinghai-Tibet plateau: evidence from $\delta^{13}C$ of spruce tree rings. Int. J. Climatol. 30 (1), 120–126.
Yu, L., Furevik, T., Otterå, O.H., Gao, Y., 2014. Modulation of the Pacific Decadal Oscillation on the summer precipitation over East China: a comparison of observations to 600-years control run of Bergen Climate Model. Clim. Dynam. 44 (1–2), 475–494.
Zhang, P., Cheng, H., Edwards, R.L., Chen, F., Wang, Y., Yang, X., Liu, J., Tan, M., Wang, X., 2008. A test of climate, sun, and culture relationships from an 1810-year Chinese cave record. Science 322, 940–942.
Zhang, Q., Gao, G., 2004. The spatial and temporal features of drought and flood disasters in the past 50 years and monitoring and warning services in China. Sci. Technol. Rev. 7, 21–24.
Zhu, J.J., Fan, Z.P., Zeng, D.H., Jiang, F.Q., Matsuzaki, T., 2003. Comparison of stand structure and growth between artificial and natural forests of *Pinus sylvestris* var. *mongolica* on sandy land. J. For. Res. 14, 103–111.
Zou, X., Zhai, P., Zhang, Q., 2005. Variations in droughts over China: 1951–2003. Geophys. Res. Lett., 32L04707